LIMNOLOGY and OCEANOGRAPHY

ASLO

Limnol. Oceanogr. 68, 2023, 2288–2304
© 2023 The Authors. *Limnology and Oceanography* published by Wiley Periodicals LLC on behalf of Association for the Sciences of Limnology and Oceanography.
doi: 10.1002/lno.12420

Mu*rK*y waters: Modeling the succession from *r* to *K* strategists (diatoms to dinoflagellates) following a nutrient release from a mining facility in Florida

Yuren Chen [1*] **Ming Li** [1] **Patricia M. Glibert** [1] **Cynthia Heil** [2]

[1]Horn Point Laboratory, University of Maryland Center for Environment Science, Cambridge, Maryland, USA
[2]Mote Marine Laboratory, Sarasota, Florida, USA

Abstract

The impacts of pulsed nutrient injections or extreme runoff events on marine ecosystems are far less studied than those associated with long-term eutrophication, particularly in regard to mechanisms regulating the response of plankton community structure. Over 800 million liters of nutrient-rich water from a fertilizer mine were discharged over a 2-week period into Tampa Bay, Florida, in 2021, providing a unique opportunity to document the plankton response. A 3D-coupled hydrodynamic biogeochemical model was developed to investigate this response and to understand the observed succession of a large, short diatom bloom followed by a secondary *Karenia brevis* bloom that lasted through the summer. The model reproduced the observed changes in nutrient concentration, total chlorophyll *a*, and diatom and *K. brevis* biomass in Tampa Bay. With a faster growth rate and spring temperature close to the optimal window of growth, diatoms had an initial competitive advantage, with 2/3 of the nutrient uptake due to ammonium and 1/3 due to nitrate. However, exhaustion of external nutrients led to the rapid decline of the diatom bloom, and the associated particular organic nitrogen sank onto the bay sediment. Enhanced sediment release of ammonium during the weeks following, and summer remineralization of dissolved organic nitrogen provided sufficient regenerated nitrogen to support slow-growing *K. brevis* that could capitalize on low nutrient conditions. Modeling analysis largely confirmed Margalef's conceptual model of *r* to *K*-selected species succession and provided additional insights into nutrient cycling supporting the initial diatom bloom and the subsequent bloom of a slow-growing harmful algal species.

Margalef (1958, 1967*a*,*b*; reviewed by Smayda 1980) developed a series of models in which the succession of phytoplankton in nutrient-rich and turbulent waters were described. Margalef's successional model builds on the notion that there is a succession of species from those that are "*r*" selected—those that are fast-growing, typically with shorter life spans, to those that are "*K*" selected that have a slower rate of growth but which tend to be longer lived. In brief, his conceptual models envisioned that in nutrient-rich waters (such as upwelling conditions), small diatoms cells should dominate the first phase of bloom response. Diatoms have a high surface/volume ratio and high potential growth rates. In the later stage of blooms, when nutrients have been depleted and stratification has been established, diatoms tend to sink out, and larger dinoflagellate species with lower growth rates predominate. In the field of plant ecology, Grime (1977) provided another species succession theory describing a three-way trade-off between organisms, known as the competitors-stress tolerators-ruderals (CSR) triangle, which described a succession from high production strategists (competitor) to stress-tolerant strategists to Ruderal species along the decrease in available nutrient resources. Since Margalef's papers, it has been shown diatoms are true photoautotrophs, while dinoflagellates have a more flexible nutrient acquisition strategy, strategies that affect biogeochemical cycling with feedback implications for growth that challenge the classic Margalef's successional models (reviewed by Glibert and Mitra 2022). Furthermore, it remains unclear if plankton response to a short pulse of intense nutrient loading can be interpreted within this theoretical framework, especially the nutrient recycling processes

*Correspondence: ychen@umces.edu

This is an open access article under the terms of the Creative Commons Attribution License, which permits use, distribution and reproduction in any medium, provided the original work is properly cited.

Additional Supporting Information may be found in the online version of this article.

Author Contribution Statement: M.L., Y.C., and P.M.G. conceived the study. Y.C. conducted the numerical model simulations. Y.C. and M.L. analyzed the model results. C.H. provided the observational data for model configuration and model-data comparison. Y.C. and M.L. wrote the original draft, and P.M.G. and C.H. reviewed and edited the draft.

that could support a succession of plankton blooms over an extended period of time.

In 2021, a major nutrient injection into Tampa Bay, Florida, occurred over 2 weeks following the breach of a holding pond of wastewater from an abandoned phosphorus (P) mining plant at Piney Point. This spring nutrient pulse provided the opportunity to observe the succession of phytoplankton taxa and to use a modeling approach to understand the underlying processes that led to a several months-long successional sequence from diatoms to the dinoflagellate *Karenia brevis* that was able to be sustained and thrive through the summer, a time when *K. brevis* typically does not bloom.

Chemical spills/releases from mining facilities or fertilizer plants pose a major threat to coastal oceans. Over the past decade, about 55 major spills/emergence releases were reported around the world, discharging hundreds of million cubic meters of wastewater and nutrients into the ocean and sensitive nearshore habitats (WISE 2022). The released nutrients stimulate primary production and may lead to cascading effects on entire marine and coastal ecosystems (Ghosh et al. 1999; Yeager et al. 2005). Furthermore, disproportionate releases of certain nutrient types can change nutrient stoichiometry in the water, favoring harmful algal species, many of which thrive in unbalanced nutrients (Glibert 2016). For example, over 41 million liters of swine wastewater was discharged into the New River estuary after the accidental rupture of a waste-holding lagoon in 1995, triggering a noxious algal bloom in the following 2 weeks (Burkholder et al. 1997). An anomalous release of phosphogypsum into the Grand Bay National Estuarine Research Reserve in 2005 resulted in a 10-fold increase in PO_4^{3-} concentration and an 18–56% increase in chlorophyll *a* (Chl *a*; Beck et al. 2018).

Similarly, stormwater runoff over polluted land or agricultural fields during flood events can bring huge amounts of pollutants and nutrients into rivers, bays, and coastal oceans over a short period of time (Paerl et al. 2006*a*,*b*; Chen et al. 2019). For example, Hurricanes Dennis, Floyd, and Irene passed through North Carolina in 1999, delivering over half of the typical annual nitrogen (N) loading in a very short time span and resulting in 3–5 times higher phytoplankton biomass over the next 6 months (Paerl et al. 2001). In particular, cryptophytes and chlorophytes responded rapidly to storm events as they have higher inherent growth rates than other taxa (Hall et al. 2013; Paerl et al. 2014). In comparison, dinoflagellates with low growth rates were susceptible to flushing during high flow conditions, but their biomass increased during moderately wet storms when higher nutrient loadings and limited flushing provided a favorable combination for their growth (Paerl et al. 2001; Hall et al. 2008). More recently, Hurricane Ian produced extensive watershed flooding and a large estuarine plume laden with nutrient and dissolved organic matter, precipitating an intense *K. brevis* bloom on the West Florida Shelf in 2022 (https://www.flickr.com/photos/myfwc/sets/72157635398013168).

Despite the previous studies, the impacts of pulsed nutrient injections due to chemical spills/emergence releases or extreme runoff events on marine ecosystems are not as well understood as those related to long-term eutrophication (Rabalais et al. 2009; Harding et al. 2015; Song et al. 2022). Although Margalef's successional conceptual models would suggest that a strong pulse of nutrients should initially favor fast-growing phytoplankton species (Margalef 1967*b*; Reynolds 1987), much is unknown about how intensive nutrient pulses affect the plankton community composition over the longer term, including a delayed response of slow-growing harmful algal species and potential long-lasting changes in marine ecosystems (Paerl et al. 2001; Valdes-Weaver et al. 2006). The fertilizer wastewater discharge into Tampa Bay in 2021 provided a unique opportunity to test ecological concepts of phytoplankton succession and biogeochemical cycling in response to a strong pulse of nutrient loading; such intense nutrient pulses are becoming more common in a warming climate featuring more extreme precipitation events (Knutson et al. 2019, 2020).

With one of the largest storages of phosphatic ore in the United States, central Florida hosts numerous P mining facilities and related phosphate (PO_4^{3-}) processing plants. The Piney Point plant, located 3 km from the shore of Tampa Bay, left a legacy of over 1.9 billion liters of such nutrient-rich disposal water (Garrett et al. 2011), creating a perilous situation prone to accidental spills/emergence releases due to both human errors or structural breaches that can occur during hurricanes and tropical storms and increasing volumes from rainy season inputs. Leakages were detected in the plastic liner in the reservoir's walls in late March 2021 (Beck et al. 2022). To avoid a large-scale collapse of the reservoir structure, an emergency release of the stacked water was authorized by the Florida Department of Environmental Protection. Over a period of 10 days, approximately 814 million liters of this water was discharged into Tampa Bay through the outfall near Port Manatee, yielding a nutrient load in this period equivalent to that normally received by the lower Tampa Bay annually (Beck et al. 2022).

To understand how the phytoplankton community responded to the nutrient release from the Piney Point event and to interpret the observed succession of diatom and blooms following the nutrient release, a coupled hydrodynamic-biogeochemical model was developed for Tampa Bay and the West Florida Shelf, using the modeling framework that was previously used to study water quality and harmful algal bloom (HABs) in Chesapeake Bay (Testa et al. 2014; Li et al. 2016; Ni et al. 2019; Ni et al. 2020; Li et al. 2021; Zhang et al. 2021; Li et al. 2022; Ni and Li 2023). Specifically, we investigated whether the rapid nutrient pulse would result in a succession of *r* to K strategists, how and whether the influx of different forms and amounts of nutrients, through various recycling pathways, would support a succession of phytoplankton taxa, and the extent to which the unusual bloom of *K. brevis* that was subsequently sustained throughout the summer months may have been supported and enhanced by this unusual nutrient load.

Methods

A 3D coupled hydrodynamic-biogeochemical model was developed to investigate the plankton response to the nutrient release

from the Piney Point plant. The hydrodynamic model is based on the Regional Ocean Modeling System (ROMS) (Shchepetkin and McWilliams 2005; Haidvogel et al. 2008) and the biogeochemical model is based on the Row Column Aesop (RCA) model (Di Toro 2001; HydroQual 2004; Isleib et al. 2007).

Hydrodynamic model (ROMS)

The ROMS model was configured to cover Tampa Bay and the West Florida Shelf, spanning 87.63°W to 80.20°W and 24.14°N to 31.95°N. An orthogonal curvilinear coordinate is used to follow the general orientation of the West Florida Shelf. There are 456 × 186 grid points in the horizontal directions, with the grid resolution ranging from ~ 800 m inside Tampa Bay ~ 3 km at the offshore boundary. A terrain-following coordinate is used in the vertical direction and consists of 21 layers. The vertical eddy viscosity and diffusivity are parameterized using the $k-\varepsilon$ turbulence closure scheme with the background value set at $10^{-6}\ \mathrm{m^2\ s^{-1}}$ (Lanerolle and Patchen 2011). The Smagorinsky parameterization is used to calculate the horizontal eddy viscosity and diffusivity (Smagorinsky 1963).

The ROMS model is driven by the atmospheric, oceanic, and riverine forcing at its boundaries. At the sea surface, the air–sea fluxes of heat and momentum are calculated with the standard bulk formula (Fairall et al. 1996; Fairall et al. 2003). Wind speed, air pressure, and heat fluxes were interpolated from the NCEP Climate Forecast System Reanalysis (CFSR) dataset (https://rda.ucar.edu/datasets/ds094.0/). River discharge, salinity, and temperature were prescribed at the boundaries of 11 major tributaries, including the Lake Tarpon Canal, Hillsborough River, Alafia River, Little Manatee River, and Manatee River in Tampa Bay. The flows were obtained from daily measurements at USGS gauging stations in the rivers (https://waterdata.usgs.gov/nwis) and the reported wastewater release (Beck et al. 2022), while daily riverine salinity and temperature data were obtained from the Coastal and Heartland National Estuary Partnership Water Atlas (CHNEP, https://chnep.wateratlas.usf.edu/).

At the offshore boundaries, the Chapman boundary condition was used for free surface elevation and the Flather boundary condition was used for the barotropic velocities (Flather 1976; Chapman 1985). The Orlanski radiation boundary condition was used for the baroclinic velocities, temperature, and salinity (Orlanski 1976). Tidal components, including the tidal elevation and barotropic velocity, were extracted from the Oregon State University global inverse tidal model TPXO8 (Egbert and Erofeeva 2002), while the subtidal surface elevation was interpolated from the fine-resolution HYCOM model for the entire Gulf of Mexico (https://www.hycom.org/data/gomu0pt04/expt-90pt1m000). Since the Loop Current may interact with the West Florida Shelf (Hetland et al. 2001; Liu et al. 2016), a buffer zone is introduced at the 10 outermost grid points near the offshore boundary, in which temperature, salinity, and baroclinic velocities in the ROMS are nudged to those produced from HYCOM. To ensure a smooth transition between the two models, the nudging coefficient increases exponentially from 0 at the innermost points in the buffer zone to 0.25 at the offshore boundary.

The ROMS model was initialized using climatological temperature and salinity values from the World Ocean Atlas (https://www.ncei.noaa.gov/products/world-ocean-atlas) and ran for a spin-up period of 1 year. The outputs from this model run were used to set the initial condition for the hindcast model run of the chemical release on 01 March 2021 and the model integration ran until 31 December 2021.

Biogeochemical HAM models (RCA-HAB)

The RCA biogeochemical module (HydroQual 2004) was hard-coupled to ROMS by importing all RCA codes and subroutines into the ROMS software system, thus enabling parallel computations (Fig. 1). RCA includes a water-column component (Isleib et al. 2007) and a two-layer sediment diagenesis model (Di Toro 2001; Brady et al. 2013). The water-column model has state variables describing dissolved inorganic nitrogen (DIN: NO_3^- and NH_4^+), dissolved inorganic phosphorus (PO_4^{3-}), dissolved silica (SiO_4^{4-}), dissolved and particulate organic forms of nitrogen and phosphorus (DON, PON, DOP, and POP) of varying levels of reactivity, three functional groups of phytoplankton, and dissolved O_2 (DO). The sediment diagenesis model has one aerobic layer and one anaerobic layer, simulating the cycling of carbon (C), N, P, Si, and DO equivalences (sulfur and methane). The water column biogeochemical model and sediment diagenesis model are coupled through the water–sediment fluxes, including particulate matter deposition from the water column and diffusive exchanges of dissolved inorganic nutrients.

In the RCA model configured for Tampa Bay and West Florida Shelf, the three major phytoplankton groups are diatoms, *K. brevis* (HAB) and cyanobacteria *Synechococcus* sp. The equations describing the temporal changes in the biomass of these plankton groups are shown below:

$$\frac{\partial P_i}{\partial t}=\begin{cases}\overbrace{G_iP_i-Rr_iP_i-Rg_iP_i{}^2-\frac{\partial w_iP_i}{\partial\sigma}}^{\text{sources/sinks}}+\overbrace{\left(-\frac{\partial uP_i}{\partial x}-\frac{\partial vP_i}{\partial y}-\frac{\partial wP_i}{\partial z}\right)}^{\text{Advection}}+\overbrace{K_h\frac{\partial^2\mathrm{P}_i}{\partial x^2}+K_h\frac{\partial^2P_i}{\partial y^2}+K_v\frac{\partial^2P_i}{\partial z^2}}^{\text{Diffusion}},\ i=1\\ G_iP_i-Rr_iP_i-Rg_iP_i{}^2+\left(-\frac{\partial uP_i}{\partial x}-\frac{\partial vP_i}{\partial y}-\frac{\partial wP_i}{\partial z}\right)+K_h\frac{\partial^2P_i}{\partial x^2}+K_h\frac{\partial^2P_i}{\partial y^2}+K_v\frac{\partial^2P_i}{\partial z^2},\ i=2\\ G_iP_i-Rr_iP_i-\left(Rg_i+Rg_{kb}\frac{P_2}{P_2+k_{kb}}\right)P_i{}^2+\left(-\frac{\partial uP_i}{\partial x}-\frac{\partial vP_i}{\partial y}-\frac{\partial wP_i}{\partial z}\right)+K_h\frac{\partial^2P_i}{\partial x^2}+K_h\frac{\partial^2P_i}{\partial y^2}+K_v\frac{\partial^2P_i}{\partial z^2},\ i=3\end{cases}\tag{1}$$

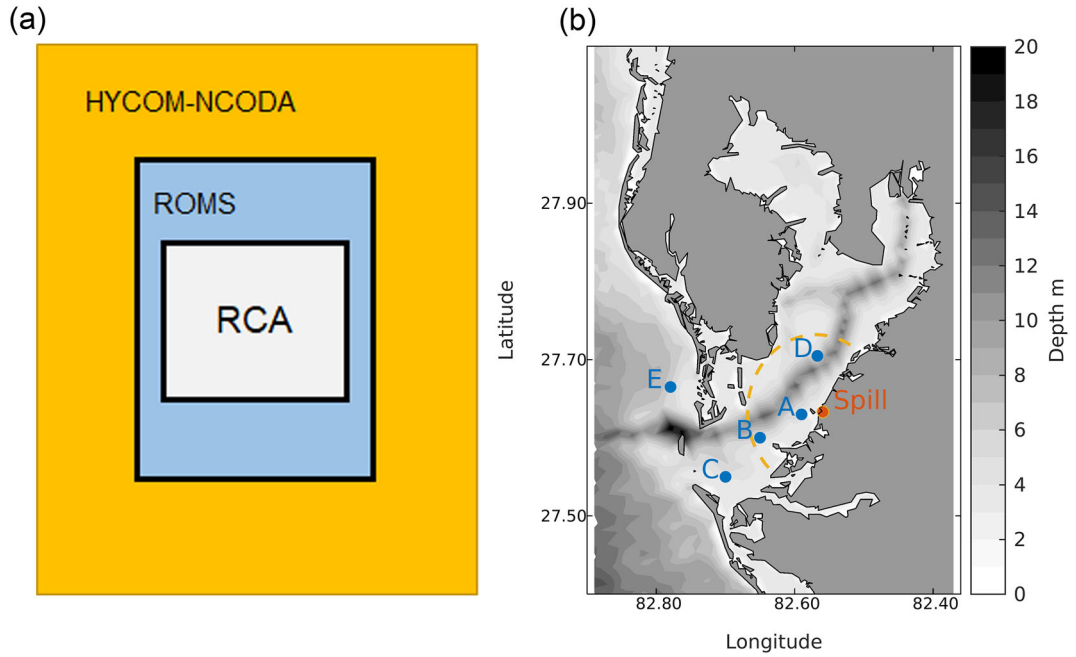

Fig. 1. (**a**) Schematic of the coupled hydrodynamic (ROMS)–biogeochemical (RCA)–HAB modeling framework that is one-way nested within the Hybrid Coordinate Ocean Model-Navy Coupled Ocean Data Assimilation global reanalysis (HYCOM-NCODA); (**b**) a map of the Tampa Bay (depths shown by the gray color scale), the location of the wastewater release outfall from the chemical plant (the orange filled circle), the location of Florida Department of Environmental Protection station Piney 6 (marked the blue dot with the label Sta. A) where nutrient and chlorophyll *a* concentration were monitored, and the locations of four stations (B, C, D, and E) selected for the following modeling analysis. The yellow dashed line marks the mid-bay area near the outfall that is used for the regional integration shown in Figs. 7 and 8.

$$G_i = G_{Ti} \cdot G_{\mathrm{par}_i} \cdot G_{Ni} \,(\cdot G_{\mathrm{Sal}}) \cdot \mu_{\max i} \tag{2}$$

where the subscripts ($i = 1$, 2, and 3) denote the biomass associated with diatoms, *K. brevis*, and *Synechococcus*, respectively. In Eq. (1), the temporal change $\partial P_i/\partial t$ at a fixed location is on the left-hand side. Terms on the right-hand side can be divided into three groups. The first group contains the source or sink terms, including the gross growth rate G_i, the respiration rate Rr_i, and mortality rate Rg_i. The loss rate due to sinking is prescribed for the diatoms with a constant sinking velocity w (Walsh et al. 2012; Iversen and Ploug 2013), while an additional mortality rate on *Synechococcus* is included based on the *K. brevis* biomass P_2. The second group includes the advective terms $(\partial uP_i/\partial x) + (\partial vP_i/\partial y) + (\partial wP_i/\partial z)$, where the velocity fields (u, v, w) are obtained from the ROMS hydrodynamic model. The third group is the turbulent diffusion term where the horizontal diffusivity K_h and vertical eddy diffusivity K_v are also calculated in ROMS. $\mu_{\max i}$ is the maximum growth rate of phytoplankton while G_{Ti} describes the growth dependence on temperature, G_{par_i} is the *P–I* curve, and G_{Ni} represents the nutrient limitation. For *K. brevis*, G_{Sal} is added to account for the salinity regulation of its growth rate according to published experimental data (Magaña and Villareal 2006).

Following the approach taken in the CoSiNE model (Chai et al. 2002; Liu et al. 2018), the nutrient limitation on phytoplankton growth is separated into two parts, one representing the NO_3^- uptake ($G_{NO_3^- i}$) and one representing NH_4^+ uptake ($G_{NH_4^+ i}$):

$$G_{Ni} = G_{NO_3^- i} + G_{NH_4^+ i} \tag{3}$$

$$r1_i = \frac{NO_3^-}{NO_3^- + k_{NO_3^- i}} \tag{4}$$

$$r2_i = \frac{NH_4^+}{NH_4^+ + k_{NH_4^+ i}} \tag{5}$$

$$G_{NO_3^- i} = \left(r1_i + r2_i, \frac{PO_4^{3-}}{PO_4^{3-} + k_{Pi}}, \frac{SiO_4^{4-}}{SiO_4^{4-} + k_{DSii}}\right) \cdot \frac{r1_i}{r1_i + r2_i} \tag{6}$$

$$G_{NH_4^+ i} = \left(r1_i + r2_i, \frac{PO_4^{3-}}{PO_4^{3-} + k_{Pi}}, \frac{SiO_4^{4-}}{SiO_4^{4-} + k_{DSii}}\right) \cdot \frac{r2_i}{r1_i + r2_i} \tag{7}$$

where the half-saturation constants for NO_3^-, NH_4^+, PO_4^{3-}, and SiO_4^{4-} are denoted by $k_{NO_3^- i}$ $k_{NH_4^+ i}$, k_{Pi}, and k_{DSii}, respectively.

The equations for NH_4^+ and NO_3^- are as follows:

$$\frac{\partial \mathrm{NH}_4^+}{\partial t} = \overbrace{r_\mathrm{L}\mathrm{LDON} + r_\mathrm{R}\mathrm{RDON} + R_{\mathrm{NH}_4^+} - U_{\mathrm{NH}_4^+} - n\mathrm{NH}_4^+}^{\text{sources/sinks}} + \overbrace{\left(-\frac{\partial u\mathrm{NH}_4^+}{\partial x} - \frac{\partial v\mathrm{NH}_4^+}{\partial y} - \frac{\partial w\mathrm{NH}_4^+}{\partial z} \right)}^{\text{Advection}} + \overbrace{K_h \frac{\partial^2 \mathrm{NH}_4^+}{\partial x^2} + K_h \frac{\partial^2 \mathrm{NH}_4^+}{\partial y^2} + K_v \frac{\partial^2 \mathrm{NH}_4^+}{\partial z^2}}^{\text{Diffusion}} \quad (8)$$

$$\frac{\partial \mathrm{NO}_3^-}{\partial t} = \overbrace{n\mathrm{NH}_4^+ - U_{\mathrm{NO}_3^-} - DNIT}^{\text{sources/sinks}} + \overbrace{\left(-\frac{\partial u\mathrm{NO}_3^-}{\partial x} - \frac{\partial v\mathrm{NO}_3^-}{\partial y} - \frac{\partial w\mathrm{NO}_3^-}{\partial z} \right)}^{\text{Advection}} + \overbrace{K_h \frac{\partial^2 \mathrm{NO}_3^-}{\partial x^2} + K_h \frac{\partial^2 \mathrm{NO}_3^-}{\partial y^2} + K_v \frac{\partial^2 \mathrm{NO}_3^-}{\partial z^2}}^{\text{Diffusion}} \quad (9)$$

where the subscripts (L and R) denote the labile and refractory form of ON. r and n refer to the remineralization and nitrification coefficients. In both equations, the temporal change at a fixed location is on the left-hand side. The source/sink terms of Eq. (8) includes the remineralization from DON (r_LLDON, r_RRDON) and regenerated NH_4^+ from phytoplankton mortality ($R_{\mathrm{NH}_4^+}$), while the loss terms are phytoplankton uptake ($U_{\mathrm{NH}_4^+}$) and nitrification ($n\mathrm{NH}_4^+$). In Eq. (9), NO_3^- gains through nitrification ($n\mathrm{NH}_4^+$) but is lost due to phytoplankton uptake ($U_{\mathrm{NO}_3^-}$) and denitrification (DNIT). In addition, NO_3^- and NH_4^+ are affected by advection and diffusion processes through the other terms on the right-hand side of Eqs. (8) and (9), such as the riverine inputs, benthic flux, and the upwelling of deep ocean nutrients. The remineralization rates of the labile and refraction dissolved organic matter (DOM) are given by

$$r_\mathrm{L} = r_\mathrm{Lt}\theta_\mathrm{rL}^{(T-20)} \frac{\mathrm{TPHYT}}{\mathrm{TPHYT} + k_\mathrm{phyt}} \quad (10)$$

$$r_\mathrm{R} = r_\mathrm{Rt}\theta_\mathrm{rR}^{(T-20)} \frac{\mathrm{TPHYT}}{\mathrm{TPHYT} + k_\mathrm{phyt}} \quad (11)$$

and the nitrification rate is given by

$$n = n_t\theta_n^{(T-20)} \frac{\mathrm{DO}}{\mathrm{DO} + k_{m\mathrm{NIT}}} \quad (12)$$

where r_Lt, r_Rt, and n_t are the rates at 20°C, and θ_rL, θ_rR, and θ_n are the temperature coefficients. TPHYT refers to the total phytoplankton biomass, k_phyt is the corresponding half-saturation coefficient, and $k_{m\mathrm{NIT}}$ is the half-saturation coefficient for nitrification.

Values of the parameters used in the RCA model were chosen according to the published literature (Testa et al. 2014; Li et al. 2016; Ni et al. 2019; Ni et al. 2020; Ni and Li 2023) as well as the previous studies on the West Florida Shelf (Walsh et al. 2003; Walsh et al. 2012). Table 1 lists the key parameters, their values, and units.

Water quality data from the CHNEP were used to set the boundary conditions at the river boundaries. More details about this data set can be found at the archive (https://chnep.wateratlas.usf.edu/), including the measurement techniques for NH_4^+ (USEPA Method 350.1), NO_3^- (APHA Method 4500-NO3F), PO_4^{3-} (APHA Method 4500-PF), and SiO_4^{4-} (USEPA Method 370.1). At the Piney Point site, the NH_4^+ and PO_4^{3-} concentrations of the outflow were set to be 210 mg L^{-1} (= 15,000 μM) and 140 mg L^{-1} (= 4516 μM) according to observations provided by the Florida Department of Environmental Protection (Beck et al. 2022). Climatological values from the World Ocean Atlas (https://www.ncei.noaa.gov/products/world-ocean-atlas) and the NEGOM cruise data (Jochens et al. 2002) were combined to prescribe the initial NO_3^-, NH_4^+, PO_4^{3-}, and dissolved Si concentrations on the shelf and their time series at the offshore boundaries. Meanwhile, the initial concentrations of DON on the shelf were estimated by cruise samples from 2007 to 2010 (Dixon et al. 2014). Inside Tampa Bay, the initial nutrient concentrations were interpolated from the CHNEP data, which almost cover the whole bay. Since observations of diatoms and *K. brevis* within Tampa Bay were limited during the spring of 2021, their initial concentrations were estimated by combining the cell count data collected by the Mote Marine Laboratory with those reported to the Fish and Wildlife Research Institute website (https://myfwc.com/research/redtide/).

Results

Short-term response—A large diatom bloom

The discharge of wastewater from the Piney Point plant began on 30 March and ceased on 09 April 2021, releasing about 180 metric tons of total N, mostly in the form of NH_4^+ (15,000 μmol L^{-1}) and little in the form of NO_3^- (0.029 μmol L^{-1}), and over 110 metric tons of P (5100 μmol L^{-1}) into lower Tampa Bay. The concentration of PO_4^{3-} reached a maximum of ~20 μmol L^{-1} near the release site (Fig. 2a). As the currents moved back and forth and dispersed the wastewater, PO_4^{3-} was distributed throughout the estuary. NH_4^+ also spread across the estuary, but a high-concentration patch (20–40 μmol L^{-1}) was mostly confined to the mid-estuary region surrounding the outfall site (Fig. 2e–h). Concentrations of NH_4^+ showed a marked decline from 10 to 15 April that was not seen in the PO_4^{3-} distributions (compare Fig. 2g,h with Fig. 2c,d). In comparison with NH_4^+, NO_3^- was mostly confined around the release site (Fig. 2i–l). Its maximum concentration was much lower than that of NH_4^+, ~4 μmol L^{-1} near the outfall, but was 2–3 orders of magnitude higher than that in the wastewater. The co-locations of high

Table 1. Part of model parameters for Diatom, *Karenia brevis*, *Synechococcus* ($i = 1, 2, 3$), and nitrogen cycling. The references for the values are labelled with lower-case superscript letters.

Name	Value	Description	Unit	References
μmax_i	[2.3, 0.8, 1.0][a–f]	Maximum growth rate	d^{-1}	a. Yoder (1979)
$Topt_i$	[24, 27, 28][a–e,g]	Optimal growth temperature	°C	b. Kaeriyama et al. (2011)
Rr_i	$krb_i \cdot G_i + kr_i \cdot \theta r^{T-20}$	Respiration rate	d^{-1}	c. Magaña and Villareal (2006)
krb_i	[0.03, 0.03, 0.03][h,i]	Growth-rate-dependent respiration coefficient	d^{-1}	d. Vargo (2009)
kr_i	[0.03, 0.03, 0.03][h,i]	Endogenous respiration rate at 20°C	d^{-1}	e. Tilney et al. (2019)
θr_i	[1.047, 1.047, 1.047][j]	Temperature coefficient for respiration		f. Kana and Glibert (1987)
Rg_i	$kgt_i \cdot \theta g_i^{T-20}$	Mortality rate	d^{-1}	g. Mackey et al. (2013)
kg_i	[0.12, 0.15, 0.12][h,i]	Mortality rate at 20°C	d^{-1}	h. Walsh et al. (2012)
θg_i	[1.047,1.047, 1.047][j]	Temperature coefficient for mortality		i. Walsh et al. (2003)
Rg_{kb}	0.5[k–m]	Maximum grazing rate by *Karenia brevis*	d^{-1}	j. This study
k_{kb}	0.01[k–m]	Half saturation constant for grazing by *K. brevis*	mg C L^{-1}	k. Jeong et al. (2005)
w_1	$w_{bas1} + w_{N1} \cdot (1 - G_{N1})^{T-20}$	Diatom sinking rate	d^{-1}	l. Glibert et al. (2009)
w_{bas1}	0.4[n]	Diatom base algal sinking rate	m d^{-1}	m. Procise (2012)
w_{N1}	0.5[n]	Diatom nutrient stressed sinking rate	m d^{-1}	n. Smayda (1971)
k_{NH4_i}	[1.5, 0.4, 0.1][h,o–r]	Half-saturation constant for ammonium	μmol L^{-1}	o. Eppley et al. (1969)
k_{NO3_i}	[0.7, 0.5, 0.2][h,o–t]	Half-saturation constant for nitrate	μmol L^{-1}	p. Romeo and Fisher (1982)
k_{P_i}	[0.5 0.18 0.014][d,h,r,u]	Half-saturation constant for phosphate	μmol L^{-1}	q. Killberg-Thoreson et al. (2014)
k_{Si_i}	[1.14, 0.0, 0.0][h]	Half-saturation constant for silicate	μmol L^{-1}	r. Timmermans et al. (2005)
r_{Lt}	0.03[v–x]	Mineralization rate of labile DON at 20°C	d^{-1}	s. Lomas and Glibert (1999)
r_R	0.001[v–x]	Mineralization rate of refractory DON at 20°C	d^{-1}	t. Glibert et al. (2016)
n_t	0.05[v–x]	Nitrification rate at 20°C	d^{-1}	u. Ou et al. (2008)
θ_{rL}	1.08[v–x]	Temperature coefficient for labile DON mineralization		v. Wang et al. (1999)
θ_{rR}	1.08[v–x]	Temperature coefficient for refractory DON mineralization		w. Zhang et al. (2021)
θ_n	1.08[v–x]	Temperature coefficient for nitrification		x. Li et al. (2022)
k_{phyt}	0.025[w,x]	Half-saturation constant for phytoplankton	mg C L^{-1}	
k_{mNIT}	1[w,x]	Half-saturation constant for nitrification oxygen limitation	mg O_2 L^{-1}	

NH_4^+ and NO_3^- patches near the outfall suggest that NO_3^- was generated by nitrification.

Since phytoplankton inside Tampa Bay are normally limited by N availability rather than P availability (Wang et al. 1999; Greening and Janicki 2006), the injection of high concentrations of NH_4^+ and NO_3^- resulted in the dominance of fast-growing diatoms (Fig. 2m–p). A large diatom bloom (with a concentration up to 1 mg C L^{-1}) developed on 10 April and its biomass continued to accumulate through 12 April at its peak, while NH_4^+ and NO_3^- declined due to nutrient uptake.

There was a phase lag in the temporal evolution of NH_4^+, NO_3^-, and diatom biomass following the nutrient release (Fig. 3), but the magnitude differed by station location. Sta. A is located close to the outfall. NH_4^+ reached a peak of 24 μmol L^{-1} at the end of the controlled release on 09 April and decreased to a low background concentration (~0.2 μmol L^{-1}) by 19 April (Fig. 3a). Although NO_3^- concentration in the wastewater was comparatively low, NO_3^- increased presumably due to nitrification, reaching its peak concentration around 10 April. Diatom biomass increased as NO_3^- and NH_4^+ became available and reached a peak bloom size of ~1 mg C L^{-1} rapidly, and decreased gradually to a background concentration of 0.3 mg C L^{-1} on 25 April. A phase lag can be noticed between the peak nutrient concentration and peak diatom biomass, but there was virtually no lag between the peaks of NH_4^+ and NO_3^- concentration. Although NH_4^+ and NO_3^- at the downstream Sta. B were considerably lower, a diatom bloom still developed there, with the maximum biomass of 0.5 mg C L^{-1} on 14 April (Fig. 3b). The diatom biomass at Sta. C near the mouth of Tampa Bay was far lower than that at Stas. A and B and a temporal response to the nutrient pulse could not be detected there (Fig. 3c).

These model predictions are in reasonable agreement with the observed nutrient concentrations and Chl *a*, as shown in Fig. 4 for station A (denoted as Piney 6 station by the Florida Department of Environmental Protection). The observed NH_4^+ concentration rapidly increased from 30 March to 09 April, with a maximum concentration of 20 μmol L^{-1}. The agreement between the model-predicted NH_4^+ and observed values includes the months of May and June, well after the initial nutrient injection, when both the observed and predicted NH_4^+ fell onto 0.2 μmol L^{-1} (Fig. 4a). The predicted NO_3^- time

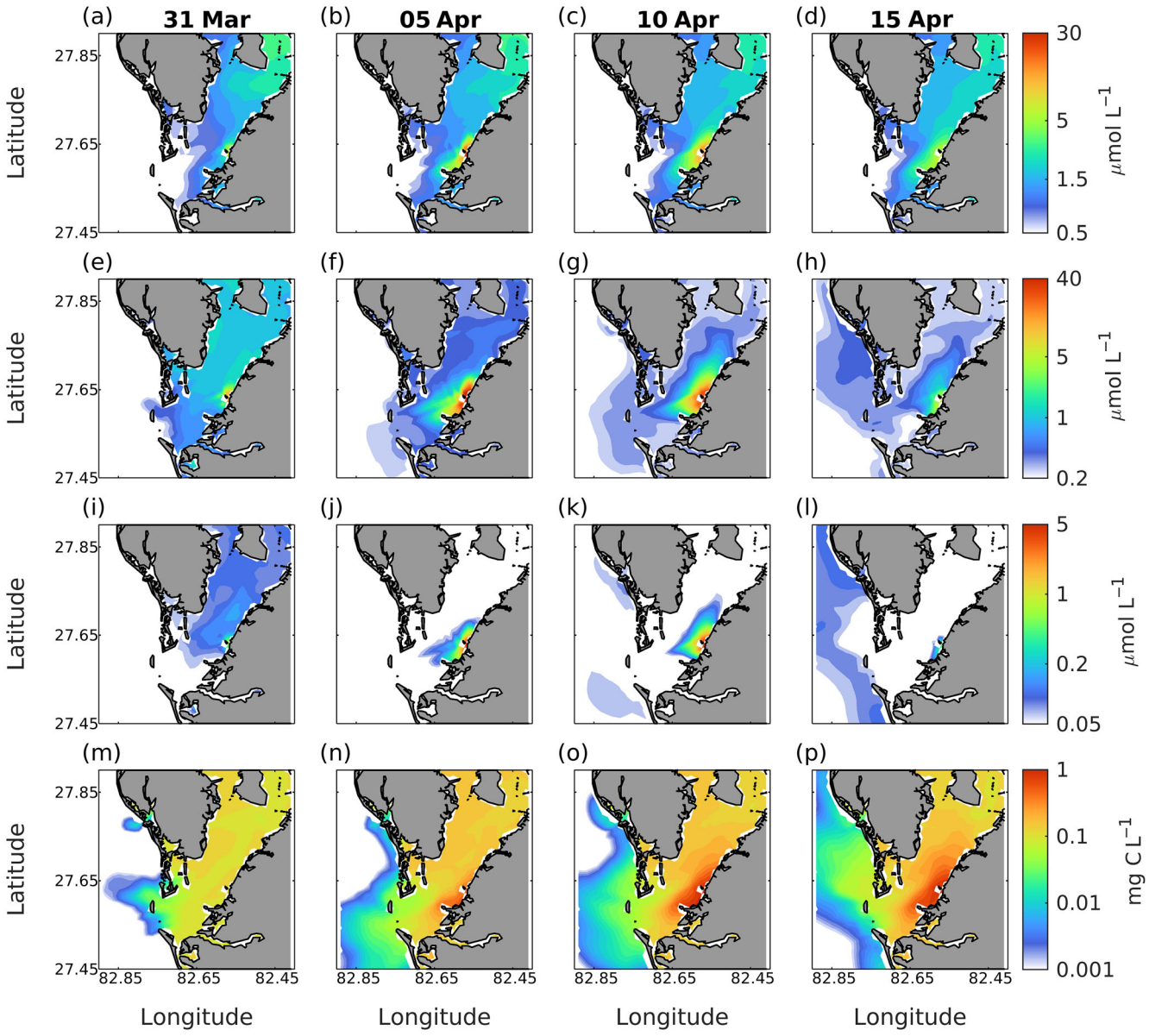

Fig. 2. Snapshots of nutrients and diatom biomass after the release. (**a**–**d**) Surface PO_4^{3-} concentration; (**e**–**h**) surface NH_4^+ concentration; (**i**–**l**) surface NO_3^- concentration; (**m**–**p**) surface diatom biomass.

series is also in good agreement with the observed NO_3^-, with a peak concentration of around 1.7 μmol L^{-1} (Fig. 4b). There was no phase lag between the peak NH_4^+ and peak NO_3^-, indicating that nitrification occurred at a fast rate. The surface NH_4^+ and NO_3^- concentrations dropped to very low levels after the diatom bloom in April, indicating that most of the nutrients discharged from the chemical release were exhausted by the beginning of May. The predicted and observed PO_4^{3-} time series are also in very good agreement, rising from an initial concentration of 2 μmol L^{-1} to a maximum of 10 μmol L^{-1} on 09 April and declining to $\sim$2 μmol L^{-1} after early May (Fig. 4c). The observed Chl *a* showed a large peak of 18 μg L^{-1} around 12 April, followed by a second peak of $\sim$10 μg L^{-1} near the end of June (Fig. 4d). The predicted Chl *a* time series is in very good agreement with the observed one, not only in terms of the bloom magnitude but also in the timing of the two blooms: the first larger peak around 12 April and the second peak around 18 June. Diatom Chl *a* accounted for $\sim$99% of the total Chl *a* between 30 March and 30 April (Fig. 4d). In contrast, *K. brevis* Chl *a* accounted for $\sim$70% of the total during the summer (01 June to 31 August). A short transition period can then be noticed between 01 May and 15 May when diatom Chl *a* decreased and *K. brevis* Chl *a* started to increase (Fig. 4d).

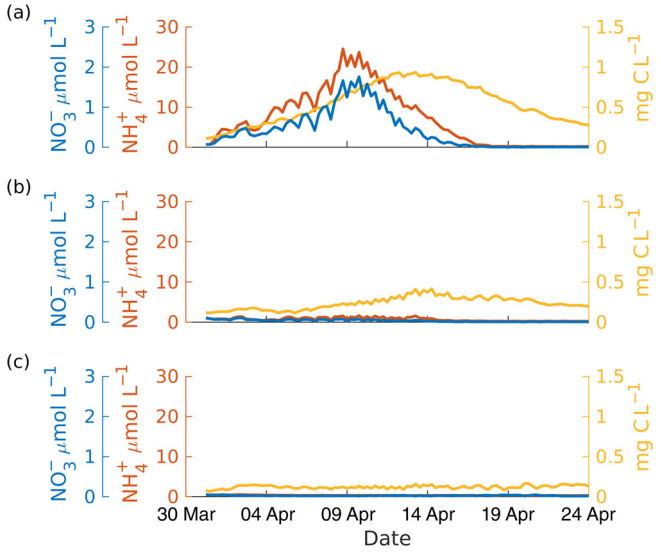

Fig. 3. Time series of surface NO_3^- (blue), NH_4^+ (red), and diatom biomass (yellow) at Sta. A (**a**) to Sta. C (**c**; see map Fig. 1).

Long-term response—A summer *K. brevis* bloom

A *K. brevis* bloom occurred ~1 month after the diatom bloom had disappeared and the surface NO_3^- and NH_4^+ concentrations dropped to low levels (~0.01 μmol L^{-1} and ~0.2 μmol L^{-1}), as shown in Fig. 4. Most of NO_3^- was depleted during the diatom bloom in April and was at near-zero concentrations except on the shelf during May–August (Fig. 5a–d). The surface NH_4^+ concentration was maintained at a level of 0.1–0.7 μmol L^{-1}, in the range of the reported half-saturation coefficient (0.4 μmol L^{-1}) for the NH_4^+ uptake by *K. brevis* (Fig. 5e–h; Table 1). More tellingly, the bottom NH_4^+ concentration was higher and in the range of 0.5–1 μmol L^{-1} (Fig. 5i–l). Given that the water column was well mixed in the shallow waters of Tampa Bay, NH_4^+ from bottom waters was constantly injected into the surface euphotic layer, providing a source of N to support *K. brevis* growth. The *K. brevis* cell density began to increase in late April, reached a peak bloom density of 10^6 cells L^{-1} in early July, and lasted until the end of August (Fig. 5m–p). Its cell density was higher at the coast and in the lower Tampa Bay, in contrast to the diatom bloom which was centered in the middle of Tampa Bay (compare Fig. 2o,p with Fig. 5o,p).

The time series in Fig. 6 provides additional insights into how NH_4^+ was regenerated and how this regenerated NH_4^+ stimulated the *K. brevis* bloom. As most of the NH_4^+ from the nutrient discharge was exhausted by 01 May, two potential sources for NH_4^+ regeneration were investigated: remineralization of DON (the first two terms on the right-hand side of Eq. 8), and the NH_4^+ release across the sediment–water interface due to the sediment diagenesis of particulate organic matter (POM) that had settled down onto the bay bottom. At Sta. A close to the outfall site, the remineralization of DON was 0.14 μmol L^{-1} d^{-1} on 01 May, decreased to

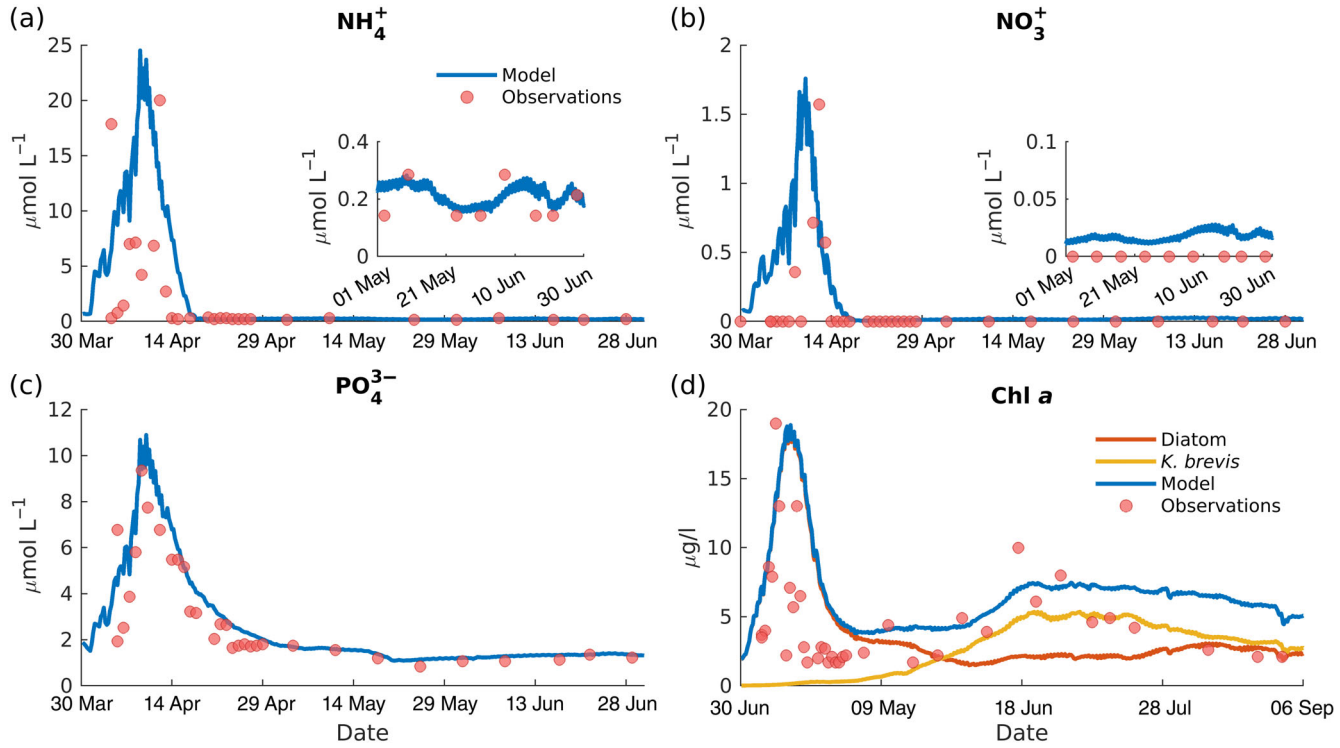

Fig. 4. NH_4^+, NO_3^-, PO_4^{3-}, and Chl *a* concentration from the model (solid lines) and observations at Sta. A (red dots).

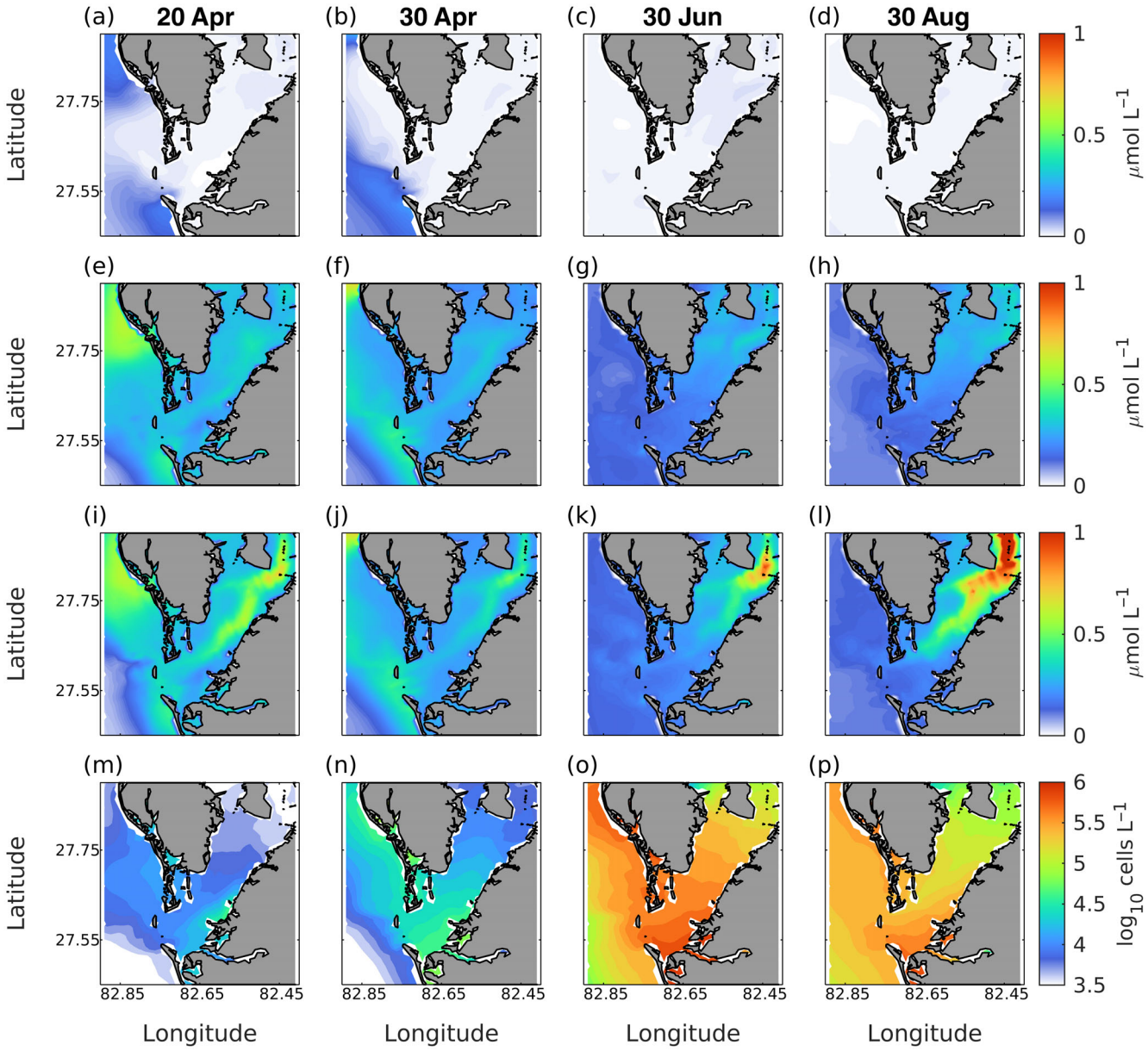

Fig. 5. Snapshots of nutrients and *Karenia brevis* biomass after the release. (**a**–**f**) Surface NO_3^- concentration; (**e**–**h**) surface NH_4^+ concentration; (**i**–**l**) bottom NH_4^+ concentration; (**m**–**p**) surface *K. brevis* biomass.

0.08 μmol L^{-1} d^{-1} around 15 May, and was maintained at this level until the end of September. The higher remineralization of DON on 1–15 May was likely associated with the decaying diatom bloom (compare Figs. 4d, 6c). In contrast, NH_4^+ efflux from the sediment was lower in May and September but considerably higher in June–August (Fig. 6a). The sediment diagenesis rate increased with temperature and was most active during the hot summer months. It is interesting to note that NH_4^+ release from the sediment was 2–3 times higher than the integrated remineralization of DON in the water column at Sta. A (Fig. 6c). A similar story with regard to NH_4^+ regeneration can be seen at Sta. C located near the mouth of Tampa Bay (Fig. 6b). At this location the sediment–water NH_4^+ flux and the remineralization of DON in the water column were of similar magnitude, as a large portion of the PON derived from the fast-sinking diatoms had already been deposited onto the bay sediment further upstream (Fig. 6d). A comparison between the NH_4^+ and *K. brevis* cell density time series suggests the NH_4^+ uptake drove the *K. brevis* bloom (Fig. 6a,b). Indeed, at Sta. A, NH_4^+ uptake increased from 0.0 to 0.3 μmol L^{-1} d^{-1} and *K. brevis* cell density increased from 0.01 to 0.16 mg C L^{-1}, while NH_4^+ declined from 0.25 μmol L^{-1} on 01 May to 0.18 μmol L^{-1} on 30 June (Fig. 6a,b). At Sta. C near the mouth of Tampa Bay, declining NH_4^+ concentration

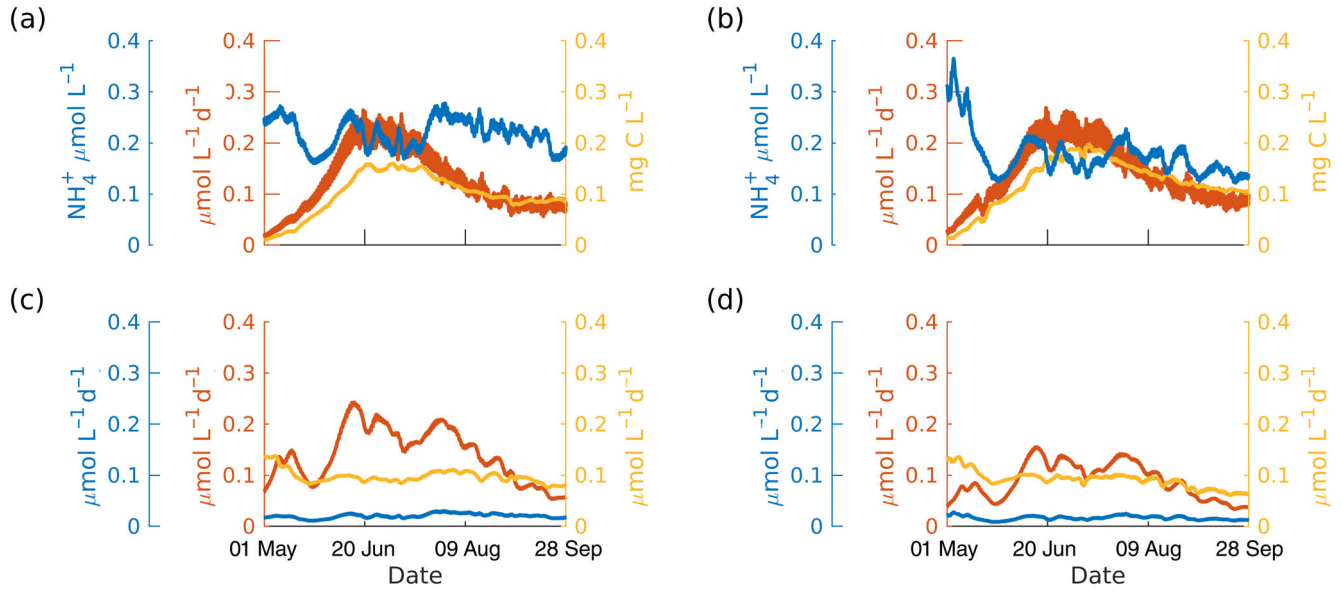

Fig. 6. (**a**–**b**) Time series of depth-averaged NH_4^+ (red), *Karenia brevis* biomass (yellow), and NH_4^+ uptake rate of *K. brevis* (blue) at Stas. A and C; (**c**–**d**) depth-averaged benthic NH_4^+ flux (red), remineralization flux (yellow), and nitrification flux (blue) at Stas A and C (Fig. 1).

and increasing *K. brevis* cell density co-occurred with increasing NH_4^+ uptake between 01 May and 30 June, affirming that *K. brevis* was supported by the regenerated NH_4^+ (Fig. 6b).

The above analysis supports the notion that NH_4^+ was regenerated from the sediment diagenesis of POM that had settled down to the seabed after the diatom bloom as well as the remineralization of DON in the water column. The nutrient release from the sediment was enhanced during the warm summer months, thereby supporting a prolonged *K. brevis* bloom that lasted from 01 May to 30 September.

Nutrient pulse release and subsequent nutrient recycling

The wastewater released from the Piney Point plant brought ~169 metric tons of NH_4^+ into Tampa Bay over a short period of 10 days, which was much larger than the accumulated riverine NH_4^+ loading of ~26 metric tons from January to August (Fig. 7a). Integrating Eq. (8) over the mid-Bay area (as shown in the area encircled by the dashed orange line in Fig. 1b) results in the following terms: the NH_4^+ influx from the Piney Point plant and transport across the semicircle boundary (including the advective and diffusive fluxes), the remineralization of DON, NH_4^+ regeneration due to phytoplankton respiration and mortality, phytoplankton utilization, and nitrification. During the initial release period (30 March to 09 April), the dominant source term in the NH_4^+ budget is the input from the Piney Point plant (Fig. 7c). The other two source terms, the remineralization of DON and NH_4^+ regeneration due to phytoplankton respiration and mortality, are much smaller. The dominant sink terms are the uptake of NH_4^+ by diatoms and the rate of nitrification. The NH_4^+ export across the outer boundary and NH_4^+ flux into the sediment is considerably smaller. As the wastewater from the Piney Point began to be released on 30 March, the rate of nitrification increased rapidly in the following week. About 46 metric tons of NH_4^+ was nitrified by the end of April, accounting for about 19% of the total NH_4^+ released into the estuary (Fig. 7e). However, the direct uptake of NH_4^+ was 2–4 times higher than the nitrification rate over the same period and the accumulated uptake amounted to ~180 metric tons. It should be noted that the accumulated DON remineralization and regeneration via respiration and mortality also became significant by the end of April, reaching ~40 metric tons.

The deposition of PON, resulting from the decaying diatom bloom, was another indirect but important sink for NH_4^+ in the water column. At the end of April, over 100 metric tons of PN were deposited to the sediment layer within the mid-bay region, while around 47 metric tons of it were bounded with sinking diatoms (Fig. 7b).

Since NH_4^+ concentrations in the water column were initially higher than those in the sediment surface layer due to the wastewater release, the diffusion between the two was a minor sink for NH_4^+ in April, but became a main source for NH_4^+ in subsequent months (Fig. 7c,d). The benthic NH_4^+ release to the water column reached the same magnitude as the total NH_4^+ load from the Piney Point plant by the end of August (Fig. 7d,f). The other two terms, the remineralization of DON and nutrient regeneration due to plankton mortality, were of a similar magnitude as the benthic NH_4^+ release. These three sources of NH_4^+ added together balanced the NH_4^+ uptake by *K. brevis*. The other two terms, nitrification and

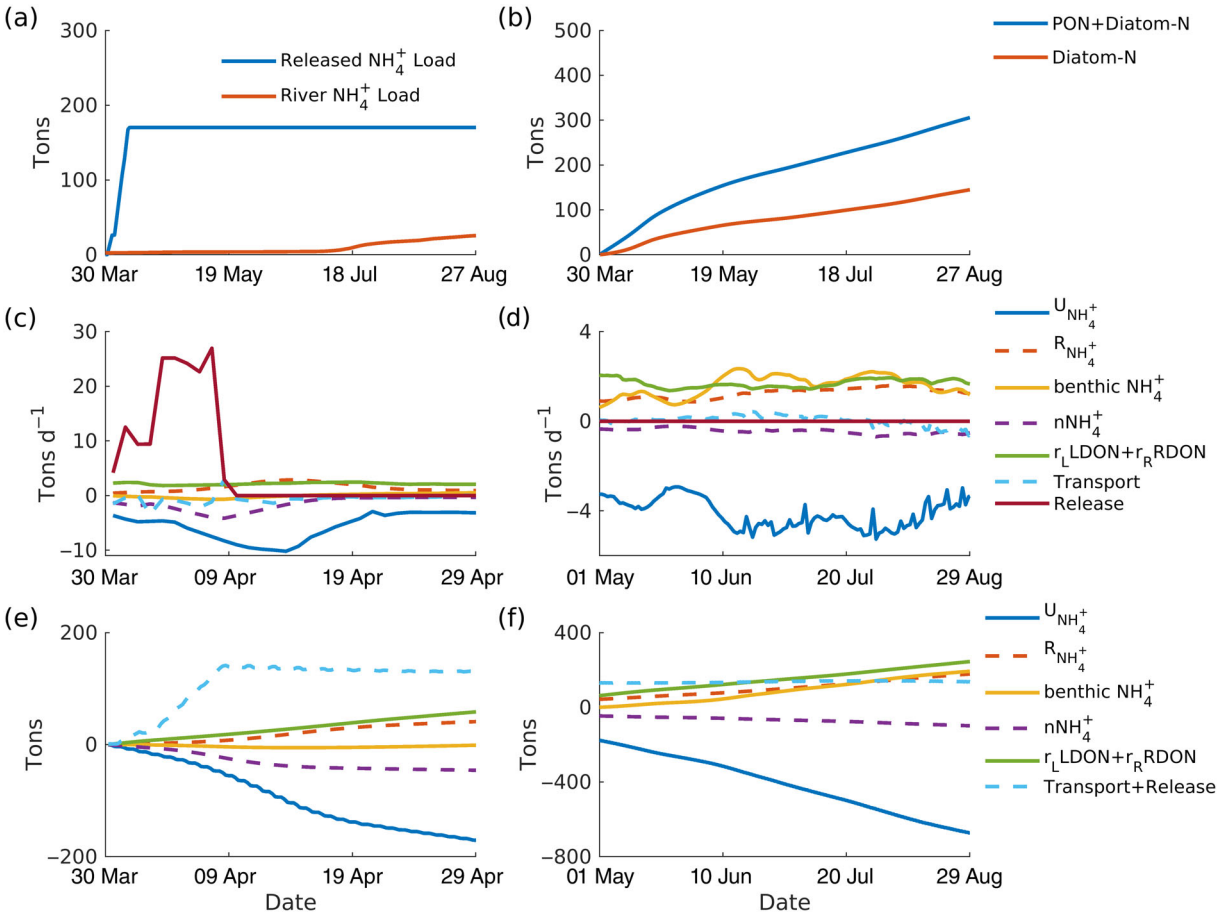

Fig. 7. Fluxes integrated over the marked region (Fig.1). (**a**) Total released (blue) and riverine (red) NH_4^+ load into Tampa Bay after 30 March; (**b**) total organic nitrogen deposition and diatom bound nitrogen deposition; (**c**,**d**) terms controlling the NH_4^+ dynamics (Eq. 8), including phytoplankton uptake ($U_{NH_4^+}$), regenerated NH_4^+ from phytoplankton mortality ($R_{NH_4^+}$), benthic release of NH_4^+, nitrification (nNH_4^+), remineralization from DON (r_LLDON, r_RRDON), hydrodynamic transport and the release from Piney Point; (**e**–**f**) same terms in (**c**–**d**), but integrated over time from 30 March.

export of NH_4^+ outside of the mid-estuary were comparatively small.

A succession of phytoplankton species

Diagnostic analysis of the plankton equations shown in Eq. (1) sheds new insights on the succession from diatom to *K. brevis* blooms. Integrating the equations for diatom P_1 and *K. brevis* P_2 for the mid-Bay area (the same area used for the NH_4^+ budget analysis) showed the relative importance of various source and sink terms.

As shown in Fig. 8a, the growth of diatoms was supported by NH_4^+ uptake but also by NO_3^- uptake. Even though the maximum NO_3^- concentration was 10 times lower than that of NH_4^+, NO_3^- uptake still contributed to about one-third of the N required to support total diatom growth. Nitrification during the initial release provided the N in oxidized form which diatoms may physiologically require (Glibert et al. 2016). Among the sink terms, the mortality was the largest, followed by the respiration and sinking of diatoms onto the bay bed. Physical transport was relatively small (diffusion was much smaller) and displayed undulations associated with the inflows and outflows in Tampa Bay. In terms of what may have caused the diatom bloom to dissipate, the rapid declines in NH_4^+ and NO_3^- concentrations reflecting NH_4^+ and NO_3^- uptake point to the exhaustion of nutrients as the main cause of the bloom termination.

Unlike the diatoms, the growth of *K. brevis* was mostly supported by NH_4^+ uptake with virtually no contribution from NO_3^- uptake (Fig. 8b). Respiration and mortality are the two domain sink terms whereas the sinking loss was nearly zero. Since the growth rate of *K. brevis* is much lower than that of diatoms (Vargo 2009), physical transport became nearly as large as the biological source and sink terms and was probably driven by the wind-driven onshore and offshore flows. Transport was negatively skewed in this period, suggesting that *K. brevis* were flushed out of the bay. This is important because it shows that the *K. brevis* bloom grew within the Bay, supported by nutrients within the Bay, and was not transported from offshore or coastal areas. The slower growth of *K. brevis* was sustained by the regenerated nutrients and was

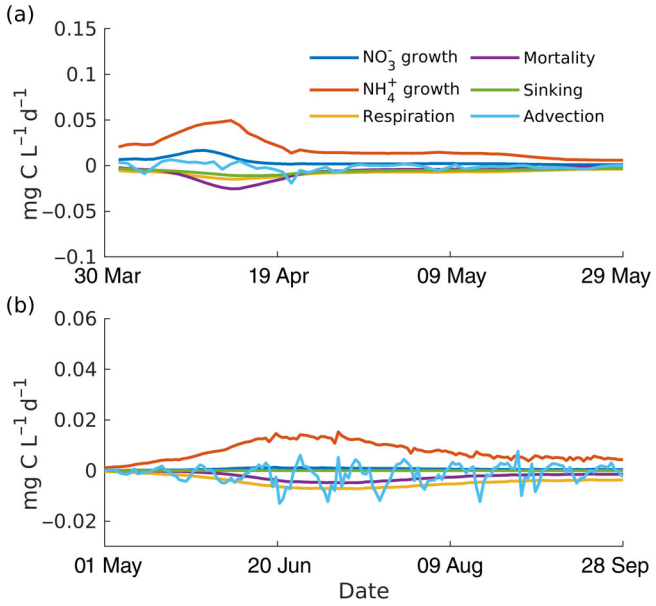

Fig. 8. Regionally and daily averaged vital terms in algal growth. (**a**,**b**) The growth and loss terms for diatoms and *K. brevis*, respectively.

able to last throughout the summer months, in contrast to the fasting-growing diatom blooms stimulated by the large source of external nutrients and the subsequent rapid bloom termination due to nutrient exhaustion.

Discussion

The three phytoplankton groups in Tampa Bay that were parameterized in this modeling study have different growth characteristics and nutrient preferences (Table 1). The mechanistic ROMS-RCA-HAB models allowed us to probe into nutrient recycling and plankton dynamics underlying the diatom and *K. brevis* successional response. First, nitrification occurred at a fast rate such that NO_3^- increased synchronously with NH_4^+ (Fig. 3). Two factors were hypothesized to contribute to the diatom's success in developing the initial bloom: (1) its higher growth rate and optimum growth window of temperature; (2) its requirement for NO_3^-. The model results largely confirmed these hypotheses. With a maximum growth rate of $2.3\,d^{-1}$, diatoms outcompeted *K. brevis* with a maximum growth rate of $0.8\,d^{-1}$ as well as that of *Synechococcus* which was assumed to have a maximum growth rate of $1.0\,d^{-1}$. Water temperature in Tampa Bay was in the range of 22–25°C in April, which is close to the diatom optimal growth temperature of 24°C. On the other hand, *K. brevis* and *Synechococcus* grow near their maximum rates when the water temperature is around 27–28°C (Vargo 2009). Diatoms have a strong preference for NO_3^-, as the half-saturation coefficient k_{NO3_1} for NO_3^- uptake ($0.7\,\mu mol\,L^{-1}$) is less than one half of the half-saturation coefficient k_{NH4_1} for NH_4^+ uptake ($1.5\,\mu mol\,L^{-1}$). The rapid nitrification and NO_3^- availability would presumably give a competitive advantage for the diatoms. Modeling diagnosis shows that NH_4^+ contributed more than NO_3^- in supporting the diatom growth (Fig. 8). This is not surprising since NH_4^+ concentration in Tampa Bay reached over $15\,\mu mol\,L^{-1}$ which was 10 times of k_{NH4_1} whereas the maximum NO_3^- concentration of $1.5\,\mu mol\,L^{-1}$ was only twice of k_{NO3_1}. The diatom bloom lasted for about 1 month or less and dissipated by the end of April as the nutrients were exhausted. The greater absolute use of NH_4^+ over NO_3^- by diatoms did not negate the importance of NO_3^- in the success of the diatoms. A recent study that used stable isotope analysis provided evidence supporting the connection between the early summer PON and the N released from the Piney Point plant (Morrison et al. 2023). A decline in the $\delta^{15}N$ values of suspended particulate material across all sampling sites suggested that the N from the Piney Point plant was incorporated into the organic particulates in May and early June, supporting the nutrient pathway identified in this modeling study.

Although a diatom–dinoflagellate sequence following nutrient enrichment was conceptualized by Margalef (Margalef 1958, 1967*a*,*b*), the development of a summer *K. brevis* bloom was surprising, for several reasons, not the least of which is that over-summering *K. brevis* blooms are unusual due to temperatures that exceed their temperature optima (Heil et al. 2022). Recently, Ahn and Glibert (2022) showed that high-temperature stress on rates of photosynthesis by the related species, *K. mikimotoi*, could be reduced by the provision of chemically reduced forms of N (NH_4^+ and urea). In this case, the succession from diatoms to dinoflagellates did not require invoking a third type of species, as represented in Grime's CSR conceptualization (Grime 1977).

The nutrient budget lends insight into how *K. brevis* blooms may have been sustained. As shown in Figs. 4 and 5, both NH_4^+ and NO_3^- in the surface waters were depleted by the end of April. Meanwhile, total PN deposition (both PON and N bound with sinking diatoms) to the sediment resulting from the diatom bloom amounted to around 55% of the total amount of NH_4^+ discharged from the Piney Point plant (Fig. 7b). Therefore, a considerable amount of N remained in the benthic layer in particulate forms after the end of the nutrient release and were later mineralized to be released as the regenerated nutrients during the warm summer months. NH_4^+ concentrations in the water column remained low, thereby benefitting the slow-growing *K. brevis*, with its lower half-saturation concentration for NH_4^+ uptake compared to that of the diatoms. The average growth rate of the *K. brevis* in the mid-bay was $0.01–0.02\,mg\,C\,L^{-1}\,d^{-1}$ (Fig. 8b), corresponding to an N uptake rate of $0.1–0.3\,\mu mol\,L^{-1}\,d^{-1}$. The sum of the regenerated N flux from remineralization of DON and sediment diagenesis ranged from 0.1 to $0.4\,\mu mol\,L^{-1}\,d^{-1}$ (Fig. 6c,d), large enough to support the *K. brevis* growth. It is also worth noting that the trend of the biomass of *K. brevis* (Fig. 6) was almost in pace with the benthic flux, both of which started to increase in late May,

peaked around mid-June, and then went down in August. Also, snapshots of deposition and benthic flux in the whole bay (Supporting Information Fig. S2) showed that areas with nutrient pulse and diatom bloom had larger benthic flux in the subsequent summer month.

In the current ROMS-RCA-HAB models a simple method was used to parameterize the mixotrophic feeding of *K. brevis* by adding a grazing term $Rg_{kb}(P_2/[P_2+k_{kb}])P_i^2$ in the equation for the cyanobacteria *Synechococcus* (Eq. 1). As *K. brevis* biomass increased, *Synechococcus* decreased (Supporting Information Fig. S3). A similar inverse relationship between the two taxa was previously shown on West Florida Shelf through signature pigment distributions (Heil et al. 2007). A more sophisticated description of mixotrophic feeding would consider the interactions of C, N, and P within a mixotrophic cell, accounting for photosynthesis, inorganic nutrient uptake and consumption and digestion of prey, as well as the potential contribution of photosynthesis from the incorporation of a kleptochloroplast (i.e., ingested photosystem; Flynn and Mitra 2009). Such a model has recently been developed for *Karlodinum veneficum* and its cryptophyte prey in the Chesapeake Bay (Li et al. 2022), and efforts are ongoing to develop such a model for *K. brevis*.

In this study dead fish killed by brevotoxin were not considered, but previous studies suggested they could generate an additional nutrient source to support *K. brevis* blooms (Heil et al. 2014). However, the close agreement between the predicted and observed NH_4^+ and Chl *a* concentration suggests that nutrient recycling due to dead fish was unlikely to be a major source of nutrients during the summer of 2021. Macroalgae is another ecosystem component that could play a role in the plankton response to the nutrient release from the Piney Point plant. Macroalgae, the cyanobacterium *Dapis pleousa*, bloomed between the diatom and *K. brevis* blooms and the decomposition of the macroalgae could provide a nutrient pathway connecting the two blooms since similar macroalgal blooms were observed following a nutrient release from Piney Point plant in 2003–2004 (Switzer et al. 2011). In addition, Tropical Storm Elsa (2021) passed through Tampa Bay during the peak of the summer *K. brevis* bloom (https://www.weather.gov/tae/2021_tropicalstorm_elsa). It could also have played a role in affecting or even promoting the summer *K. brevis* bloom and fish kills, either through enhanced water-column mixing and nutrient recycling or additional nutrient flows from the watershed. However, as an early-season Category 1 hurricane, the post-storm flood into Tampa Bay was relatively small.

The modeling study of the diatom and *K. brevis* response to the wastewater release in Tampa Bay offers a comparison with the extensive observational analysis of phytoplankton community response to tropical storms in the Neuse River estuary and Pamlico Sound (Paerl et al. 2018). The short-term response in both systems seems to fit well with Margalef's succession model that favors fast-growing species: diatoms in the Tampa Bay and cryptophytes and chlorophytes in the Neuse River. Although diatoms also have fast growth rates in the Neuse River-Pamlico Sound, they constitute less than 20% of phytoplankton biomass which may explain their relatively muted response to storms. Furthermore, there are differences between the two systems and two types of pulsed nutrient loadings that should be noted. Although the flushing time was a key parameter in regulating phytoplankton biomass accumulation in the Neuse River, it was not an important factor in Tampa Bay since the large nutrient loading was delivered by extremely high nutrient concentration and relatively low flow discharge rate.

Conclusions

In summary, the plankton response to the nutrient event from the Piney Point plant can be divided into three phases (Fig. 9). In the first phase, intensive effluent rapidly raised the

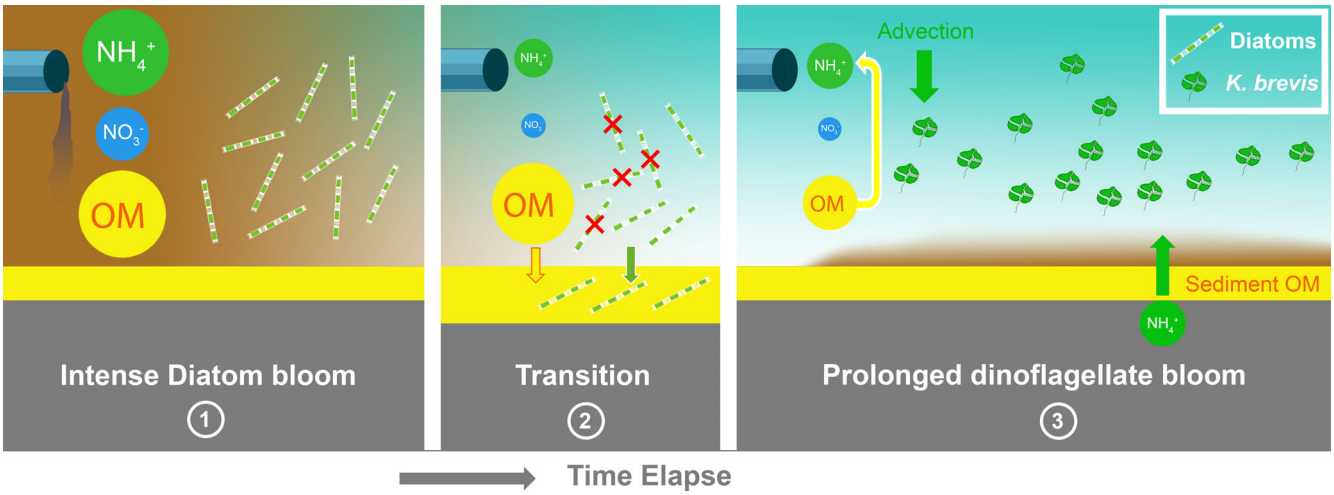

Fig. 9. A schematic diagram of the phytoplankton group succession after a massive nutrient input event.

nutrient concentration near the outfall and triggered a bloom of fast-growing diatom species. As a response to this large NH_4^+ influx, local nitrification flux also increased and resulted in increasing NO_3^-, which would provide the required NO_3^- for diatom metabolism and growth. In the second phase, nutrient concentrations dropped as the diatom exhausted the external input of nutrients. Species with higher nutrient affinity and slower growth rate benefit from the resulting relatively oligotrophic environment. A more moderate but prolonged bloom was able to develop with a moderate amount of generated nutrients. POM stored in the sediments provided an additional source for the second bloom through remineralization and benthic flux. Compared with a previous study on the N cycle in the bay (Bronk et al. 2014), our model may actually underestimate the remineralization flux.

The succession of species herein followed the general conceptual model of *r* to *K*-selected species sequence predicted by Margalef (Margalef 1958, 1967*a*,*b*). This study supports his descriptive sequence through a detailed analysis of the physiological, biogeochemical, and physical processes. The early descriptions of phytoplankton succession in relation to nutrient supply (Margalef 1958, 1967*a*,*b*), which was initially developed in the context of upwelling systems may be as common in aquatic systems receiving intensive nutrient injections from wastewater releases or storm events. These results also underscore that from the perspective of management response to such events, the initial response should not be taken as the only ecosystem response, as lagged responses may be as important from a human health or ecosystem health perspective. Moreover, the enduring consequences of this incident can provide valuable lessons for similar facilities worldwide. Most retired phosphorus fertilizer plants pose significant risks to the surrounding environment due to toxic wastewater and radioactive byproducts, but the level of investment in research and management efforts remains insufficient (Nelson et al. 2021). As such, proactive measures and stronger oversight are necessary for businesses that even continue to operate as usual, to prevent taxpayers and the environment from bearing the external costs of industry.

Data availability statement

Model output is available at https://doi.org/10.5281/zenodo.7532767.

References

Ahn, S. H., and P. M. Glibert. 2022. Shining light on photosynthesis in the harmful dinoflagellate *Karenia mikimotoi*: Responses to short-term changes in temperature, nitrogen form, and availability. Phycology **2**: 30–44. doi:10.3390/phycology2010002

Beck, M. W., K. Cressman, C. Griffin, and J. Caffrey. 2018. Water quality trends following anomalous phosphorus inputs to Grand Bay, Mississippi, USA. Gulf Caribb. Res. **29**: 1–14. doi:10.18785/gcr.2901.02

Beck, M. W., and others. 2022. Initial estuarine response to inorganic nutrient inputs from a legacy mining facility adjacent to Tampa Bay, Florida. Mar. Pollut. Bull. **178**: 113598. doi:10.1016/j.marpolbul.2022.113598

Brady, D. C., J. M. Testa, D. M. Di Toro, W. R. Boynton, and W. M. Kemp. 2013. Sediment flux modeling: Calibration and application for coastal systems. Estuar. Coast. Shelf Sci. **117**: 107–124. doi:10.1016/j.ecss.2012.11.003

Bronk, D. A., and others. 2014. Nitrogen uptake and regeneration (ammonium regeneration, nitrification and photoproduction) in waters of the West Florida Shelf prone to blooms of *Karenia brevis*. Harmful Algae **38**: 50–62. doi:10.1016/j.hal.2014.04.007

Burkholder, J. M., and others. 1997. Impacts to a coastal river and estuary from rupture of a large swine waste holding lagoon. J. Environ. Qual. **26**: 1451–1466. doi:10.2134/jeq1997.00472425002600060003x

Chai, F., R. C. Dugdale, T. H. Peng, F. P. Wilkerson, and R. T. Barber. 2002. One-dimensional ecosystem model of the equatorial Pacific upwelling system. Part I: Model development and silicon and nitrogen cycle. Deep Sea Res. II Topic. Stud. Oceanogr. **49**: 2713–2745. doi:10.1016/S0967-0645(02)00055-3

Chapman, D. C. 1985. Numerical treatment of cross-shelf open boundaries in a barotropic coastal ocean model. J. Phys. Oceanogr. **15**: 1060–1075. doi:10.1175/1520-0485(1985)015<1060:Ntocso>2.0.Co;2

Chen, S., and others. 2019. Hurricane pulses: Small watershed exports of dissolved nutrients and organic matter during large storms in the Southeastern USA. Sci. Total Environ. **689**: 232–244. doi:10.1016/j.scitotenv.2019.06.351

Di Toro, D. M. 2001. Sediment flux modeling. Wiley.

Dixon, L. K., G. J. Kirkpatrick, E. R. Hall, and A. Nissanka. 2014. Nitrogen, phosphorus and silica on the West Florida Shelf: Patterns and relationships with *Karenia* spp. occurrence. Harmful Algae **38**: 8–19. doi:10.1016/j.hal.2014.07.001

Egbert, G. D., and S. Y. Erofeeva. 2002. Efficient inverse modeling of barotropic ocean tides. J. Atmos. Oceanic Tech. **19**: 183–204. doi:10.1175/1520-0426(2002)019<0183:Eimobo>2.0.Co;2

Eppley, R. W., J. N. Rogers, and J. J. McCarthy. 1969. Half-saturation constants for uptake of nitrate and ammonium by marine phytoplankton. Limnol. Oceanogr. **14**: 912–920. doi:10.4319/lo.1969.14.6.0912

Fairall, C. W., E. F. Bradley, D. P. Rogers, J. B. Edson, and G. S. Young. 1996. Bulk parameterization of air–sea fluxes for tropical ocean-global atmosphere coupled-ocean atmosphere response experiment. J. Geophys. Res. Oceans **101**: 3747–3764. doi:10.1029/95JC03205

Fairall, C. W., E. F. Bradley, J. E. Hare, A. A. Grachev, and J. B. Edson. 2003. Bulk parameterization of air–sea fluxes: Uptakes and verification for the COARE algorithm.

J. Climate **16**: 571–591. doi:10.1175/1520-0442(2003)016<0571:Bpoasf>2.0.Co;2

Flather, R. A. 1976. A tidal model of the north-west European continental shelf. Mém. Soc. R. Sci. Liège. **10**: 141–164.

Flynn, K. J., and A. Mitra. 2009. Building the "perfect beast": Modelling mixotrophic plankton. J. Plankton Res. **31**: 965–992. doi:10.1093/plankt/fbp044

Garrett, M., J. Wolny, E. Truby, C. Heil, and C. Kovach. 2011. Harmful algal bloom species and phosphate-processing effluent: Field and laboratory studies. Mar. Pollut. Bull. **62**: 596–601. doi:10.1016/j.marpolbul.2010.11.017

Ghosh, M., K. V. R. Prasad, S. K. Mehta, and J. P. Gaur. 1999. Response of a natural phytoplankton assemblage to pulsed supply of phosphorus in semicontinuous cultures. Ann. Limnol. Int. J. Limnol. **35**: 23–29. doi:10.1051/limn/1999008

Glibert, P. M. 2016. Margalef revisited: A new phytoplankton mandala incorporating twelve dimensions, including nutritional physiology. Harmful Algae **55**: 25–30. doi:10.1016/j.hal.2016.01.008

Glibert, P. M., J. M. Burkholder, T. M. Kana, J. Alexander, H. Skelton, and C. Shilling. 2009. Grazing by *Karenia brevis* on *Synechococcus* enhances its growth rate and may help to sustain blooms. Aquat. Microb. Ecol. **55**: 17–30. doi:10.3354/ame01279

Glibert, P. M., and others. 2016. Pluses and minuses of ammonium and nitrate uptake and assimilation by phytoplankton and implications for productivity and community composition, with emphasis on nitrogen-enriched conditions. Limnol. Oceanogr. **61**: 165–197. doi:10.1002/lno.10203

Glibert, P. M., and A. Mitra. 2022. From webs, loops, shunts, and pumps to microbial multitasking: Evolving concepts of marine microbial ecology, the mixoplankton paradigm, and implications for a future ocean. Limnol. Oceanogr. **67**: 585–597. doi:10.1002/lno.12018

Greening, H., and A. Janicki. 2006. Toward reversal of eutrophic conditions in a subtropical estuary: Water quality and seagrass response to nitrogen loading reductions in Tampa Bay, Florida, USA. Environ. Manag. **38**: 163–178. doi:10.1007/s00267-005-0079-4

Grime, J. P. 1977. Evidence for the existence of three primary strategies in plants and its relevance to ecological and evolutionary theory. Am. Nat. **111**: 1169–1194.

Haidvogel, D. B., and others. 2008. Ocean forecasting in terrain-following coordinates: Formulation and skill assessment of the Regional Ocean Modeling System. J. Comput. Phys. **227**: 3595–3624. doi:10.1016/j.jcp.2007.06.016

Hall, N. S., and others. 2008. Environmental factors contributing to the development and demise of a toxic dinoflagellate (*Karlodinium veneficum*) bloom in a shallow, eutrophic, lagoonal estuary. Estuar. Coast. **31**: 402–418. doi:10.1007/s12237-008-9035-x

Hall, N. S., H. W. Paerl, B. L. Peierls, A. C. Whipple, and K. L. Rossignol. 2013. Effects of climatic variability on phytoplankton community structure and bloom development in the eutrophic, microtidal, New River Estuary, North Carolina, USA. Estuar. Coast. Shelf Sci. **117**: 70–82. doi:10.1016/j.ecss.2012.10.004

Harding, L. W., and others. 2015. Long-term trends of nutrients and phytoplankton in Chesapeake Bay. Estuar. Coast. **39**: 664–681. doi:10.1007/s12237-015-0023-7

Heil, C. A., M. Revilla, P. M. Glibert, and S. Murasko. 2007. Nutrient quality drives differential phytoplankton community composition on the southwest Florida shelf. Limnol. Oceanogr. **52**: 1067–1078. doi:10.4319/lo.2007.52.3.1067

Heil, C. A., and others. 2014. Blooms of *Karenia brevis* (Davis) G. Hansen & Ø. Moestrup on the West Florida Shelf: Nutrient sources and potential management strategies based on a multi-year regional study. Harmful Algae **38**: 127–140. doi:10.1016/j.hal.2014.07.016

Heil, C. A., and others. 2022. Termination patterns of *Karenia brevis* blooms in the eastern Gulf of Mexico. Proc. Int. Conf. Harmful Algal. **2022**: 64–69. doi:10.5281/zenodo.7034923

Hetland, R., Y. Hsueh, and D. L. Yuan. 2001. On the decay of a baroclinic jet flowing along a continental slope. J. Geophys. Res. Oceans **106**: 19797–19807. doi:10.1029/2000jc000254

HydroQual, I. 2004. User's guide for RCA, 3rd ed. HydroQual.

Isleib, R. R. P. E., J. J. Fitzpatrick, and J. Mueller. 2007. The development of a nitrogen control plan for a highly urbanized tidal embayment. Proc. Water Environ. Fed. **2007**: 296–320. doi:10.2175/193864707786619152

Iversen, M. H., and H. Ploug. 2013. Temperature effects on carbon-specific respiration rate and sinking velocity of diatom aggregates—Potential implications for deep ocean export processes. Biogeosciences **10**: 4073–4085. doi:10.5194/bg-10-4073-2013

Jeong, H. J., and others. 2005. Feeding by red-tide dinoflagellates on the cyanobacterium *Synechococcus*. Aquat. Microb. Ecol. **41**: 131–143. doi:10.3354/ame041131

Jochens, A. E., S. F. DiMarco, J. W. D. Nowlin, R. O. Reid, and M. C. Kennicutt II 2002. Northeastern gulf of Mexico chemical oceanography and hydrography study: Synthesis report. OCS Study MMS 2002-055: 586.

Kaeriyama, H., and others. 2011. Effects of temperature and irradiance on growth of strains belonging to seven *Skeletonema* species isolated from Dokai Bay, southern Japan. Eur. J. Phycol. **46**: 113–124. doi:10.1080/09670262.2011.565128

Kana, T. M., and P. M. Glibert. 1987. Effect of irradiances up to 2000 μE m^{-2} s^{-1} on marine *Synechococcus* WH7803—I. Growth, pigmentation, and cell composition. Deep Sea Res. A Oceanogr. Res. Pap. **34**: 479–495. doi:10.1016/0198-0149(87)90001-X

Killberg-Thoreson, L., M. R. Mulholland, C. A. Heil, M. P. Sanderson, J. M. O'Neil, and D. A. Bronk. 2014. Nitrogen uptake kinetics in field populations and cultured strains of *Karenia brevis*. Harmful Algae **38**: 73–85. doi:10.1016/j.hal.2014.04.008

Knutson, T., and others. 2019. Tropical cyclones and climate change assessment: Part I: Detection and attribution. Bull. Am. Meteorol. Soc. **100**: 1987–2007. doi:10.1175/bams-d-18-0189.1

Knutson, T., and others. 2020. Tropical cyclones and climate change assessment: Part II: Projected response to anthropogenic warming. Bull. Am. Meteorol. Soc. **101**: E303–E322. doi:10.1175/bams-d-18-0194.1

Lanerolle, L. W. J., and R. C. Patchen. 2011. The design, calibration and validation of a coupled numerical ocean modeling system for the west Florida shelf. NOAA Technical Report NOS CS 31. Coast Survey Development Lab.

Li, M., and others. 2016. What drives interannual variability of hypoxia in Chesapeake Bay: Climate forcing versus nutrient loading? Geophys. Res. Lett. **43**: 2127–2134. doi:10.1002/2015gl067334

Li, M., F. Zhang, and P. M. Glibert. 2021. Seasonal life strategy of *Prorocentrum minimum* in Chesapeake Bay, USA: Validation of the role of physical transport using a coupled physical-biogeochemical-harmful algal bloom model. Limnol. Oceanogr. **66**: 3873–3886. doi:10.1002/lno.11925

Li, M., Y. Chen, F. Zhang, Y. Song, P. M. Glibert, and D. K. Stoecker. 2022. A three-dimensional mixotrophic model of *Karlodinium veneficum* blooms for a eutrophic estuary. Harmful Algae **113**: 102203. doi:10.1016/j.hal.2022.102203

Liu, Y. G., R. H. Weisberg, J. M. Lenes, L. Y. Zheng, K. Hubbard, and J. J. Walsh. 2016. Offshore forcing on the "pressure point" of the West Florida Shelf: Anomalous upwelling and its influence on harmful algal blooms. J. Geophys. Res. Oceans **121**: 5501–5515. doi:10.1002/2016jc011938

Liu, Q. Q., and others. 2018. San Francisco Bay nutrients and plankton dynamics as simulated by a coupled hydrodynamic-ecosystem model. Cont. Shelf Res. **161**: 29–48. doi:10.1016/j.csr.2018.03.008

Lomas, M. W., and P. M. Glibert. 1999. Temperature regulation of nitrate uptake: A novel hypothesis about nitrate uptake and reduction in cool-water diatoms. Limnol. Oceanogr. **44**: 556–572. doi:10.4319/lo.1999.44.3.0556

Mackey, K. R., and others. 2013. Effect of temperature on photosynthesis and growth in marine *Synechococcus* spp. Plant Physiol. **163**: 815–829. doi:10.1104/pp.113.221937

Magaña, H. A., and T. A. Villareal. 2006. The effect of environmental factors on the growth rate of *Karenia brevis* (Davis) G. Hansen and Moestrup. Harmful Algae **5**: 192–198. doi:10.1016/j.hal.2005.07.003

Margalef, R. 1958. Temporal succession and spatial heterogeneity in phytoplankton, p. 323–350. *In* A. A. Buzzati-Traverso [ed.], Perspectives in marine biology. University of California Press.

Margalef, R. 1967*a*. The food web in the pelagic environment. Helgoländ. Wiss. Meer. **15**: 548–559. doi:10.1007/BF01618650

Margalef, R. 1967*b*. Succession in marine populations. p. 137–188. *In* L. Chandra and R. Vira [eds.], Advancing frontiers of plant science. Impex India.

Morrison, E. S., and others. 2023. The response of Tampa Bay to a legacy mining nutrient release in the year following the event. Front. Ecol. Evol. **11**: 1144778. doi:10.3389/fevo.2023.1144778

Nelson, N. G., M. L. Cuchiara, C. O. Hendren, J. L. Jones, and A. M. Marshall. 2021. Hazardous spills at retired fertilizer manufacturing plants will continue to occur in the absence of scientific innovation and regulatory enforcement. Environ. Sci. Technol. **55**: 16267–16269. doi:10.1021/acs.est.1c05311

Ni, W., M. Li, A. C. Ross, and R. G. Najjar. 2019. Large projected decline in dissolved oxygen in a eutrophic estuary due to climate change. J. Geophys. Res. Oceans **124**: 8271–8289. doi:10.1029/2019jc015274

Ni, W., M. Li, and J. M. Testa. 2020. Discerning effects of warming, sea level rise and nutrient management on long-term hypoxia trends in Chesapeake Bay. Sci. Total Environ. **737**: 139717. doi:10.1016/j.scitotenv.2020.139717

Ni, W., and M. Li. 2023. What drove the nonlinear hypoxia response to nutrient loading in Chesapeake Bay during the 20th century? Sci. Total Environ. **861**: 160650. doi:10.1016/j.scitotenv.2022.160650

Orlanski, I. 1976. A simple boundary condition for unbounded hyperbolic flows. J. Comput. Phys. **21**: 251–269. doi:10.1016/0021-9991(76)90023-1

Ou, L., D. Wang, B. Huang, H. Hong, Y. Qi, and S. Lu. 2008. Comparative study of phosphorus strategies of three typical harmful algae in Chinese coastal waters. J. Plankton Res. **30**: 1007–1017. doi:10.1093/plankt/fbn058

Paerl, H. W., and others. 2001. Ecosystem impacts of three sequential hurricanes (Dennis, Floyd, and Irene) on the United States' largest lagoonal estuary, Pamlico sound, NC. Proc. Natl. Acad. Sci. U. S. A. **98**: 5655–5660. doi:10.1073/pnas.101097398

Paerl, H. W., L. M. Valdes, B. L. Peierls, J. E. Adolf, and L. W. Harding. 2006*a*. Anthropogenic and climatic influences on the eutrophication of large estuarine ecosystems. Limnol. Oceanogr. **51**: 448–462. doi:10.4319/lo.2006.51.1_part_2.0448

Paerl, H. W., and others. 2006*b*. Ecological response to hurricane events in the Pamlico Sound system, North Carolina, and implications for assessment and management in a regime of increased frequency. Estuar. Coast. **29**: 1033–1045. doi:10.1007/Bf02798666

Paerl, H. W., N. S. Hall, B. L. Peierls, K. L. Rossignol, and A. R. Joyner. 2014. Hydrologic variability and its control of phytoplankton community structure and function in two shallow, coastal, lagoonal ecosystems: The Neuse and New River Estuaries, North Carolina, USA. Estuar. Coast. **37**: 31–45. doi:10.1007/s12237-013-9686-0

Paerl, H. W., and others. 2018. Two decades of tropical cyclone impacts on North Carolina's estuarine carbon, nutrient and phytoplankton dynamics: Implications for biogeochemical cycling and water quality in a stormier world. Biogeochemistry **141**: 307–332. doi:10.1007/s10533-018-0438-x

Procise, L. A. 2012. Grazing on *Synechococcus* spp. by the red-tide dinoflagellate *Karenia brevis*: Implications for bloom dynamics in the Gulf of Mexico. Ph.D. thesis. Old Dominion Univ. doi:10.25777/jy09-7349

Rabalais, N. N., R. E. Turner, R. J. Diaz, and D. Justic. 2009. Global change and eutrophication of coastal waters. ICES J. Mar. Sci. **66**: 1528–1537. doi:10.1093/icesjms/fsp047

Reynolds, C. S. 1987. The response of phytoplankton communities to changing lake environments. Swiss J. Hydrol. **49**: 220–236. doi:10.1007/Bf02538504

Romeo, A. J., and N. S. Fisher. 1982. Intraspecific comparisons of nitrate uptake in three marine diatoms. J. Phycol. **18**: 220–225. doi:10.1111/j.1529-8817.1982.tb03177.x

Shchepetkin, A. F., and J. C. McWilliams. 2005. The regional oceanic modeling system (ROMS): A split-explicit, free-surface, topography-following-coordinate oceanic model. Ocean Model. **9**: 347–404. doi:10.1016/j.ocemod.2004.08.002

Smagorinsky, J. 1963. General circulation experiments with the primitive equations. Mon. Weather Rev. **91**: 99–164. doi:10.1175/1520-0493(1963)091<0099:Gcewtp>2.3.Co;2

Smayda, T. J. 1971. Normal and accelerated sinking of phytoplankton in the sea. Mar. Geol. **11**: 105–122. doi:10.1016/0025-3227(71)90070-3

Smayda, T. J. 1980. Phytoplankton species succession, p. 493–570. *In* I. Morris [ed.], The physiological ecology of phytoplakton. Univ. Chicago Press.

Song, Y., and others. 2022. Water quality shifts the dominant phytoplankton group from diatoms to dinoflagellates in the coastal ecosystem of the Bohai Bay. Mar. Pollut. Bull. **183**: 114078. doi:10.1016/j.marpolbul.2022.114078

Switzer, T. S., Tyler-Jedlund, A. J., Rogers, K. R., Grier, H., McMichael Jr, R. H., Fox, S. 2011. Response of estuarine nekton to the regulated discharge of treated phosphate-production process water. Florida Fish and Wildlife Conservation Commission, Fish and Wildlife Research Institute.

Testa, J. M., and others. 2014. Quantifying the effects of nutrient loading on dissolved O_2 cycling and hypoxia in Chesapeake Bay using a coupled hydrodynamic–biogeochemical model. J. Mar. Syst. **139**: 139–158. doi:10.1016/j.jmarsys.2014.05.018

Tilney, C. L., S. Shankar, K. A. Hubbard, and A. A. Corcoran. 2019. Is *Karenia brevis* really a low-light-adapted species? Harmful Algae **90**: 101709. doi:10.1016/j.hal.2019.101709

Timmermans, K. R., B. van der Wagt, M. J. W. Veldhuis, A. Maatman, and H. J. W. de Baar. 2005. Physiological responses of three species of marine pico-phytoplankton to ammonium, phosphate, iron and light limitation. J. Sea Res. **53**: 109–120. doi:10.1016/j.seares.2004.05.003

Valdes-Weaver, L. M., M. F. Piehler, J. L. Pinckney, K. E. Howe, K. Rossignol, and H. W. Paerl. 2006. Long-term temporal and spatial trends in phytoplankton biomass and class-level taxonomic composition in the hydrologically variable Neuse-Pamlico estuarine continuum, North Carolina, U.S.A. Limnol. Oceanogr. **51**: 1410–1420. doi:10.4319/lo.2006.51.3.1410

Vargo, G. A. 2009. A brief summary of the physiology and ecology of *Karenia brevis* Davis (G. Hansen and Moestrup comb. nov.) red tides on the West Florida Shelf and of hypotheses posed for their initiation, growth, maintenance, and termination. Harmful Algae **8**: 573–584. doi:10.1016/j.hal.2008.11.002

Walsh, J. J., and others. 2003. Phytoplankton response to intrusions of slope water on the West Florida shelf: Models and observations. J. Geophys. Res. Oceans **108**: 3190. doi:10.1029/2002jc001406

Walsh, J. J., B. Penta, D. A. Dieterle, and W. P. Bissett. 2012. Predictive ecological modeling of harmful algal blooms. Hum. Ecol. Risk Assess. Int. J. **7**: 1369–1383. doi:10.1080/20018091095069

Wang, P. F., J. Martin, and G. Morrison. 1999. Water quality and eutrophication in Tampa Bay, Florida. Estuar. Coast. Shelf Sci. **49**: 1–20. doi:10.1006/ecss.1999.0490

WISE. 2022. Chronology of major tailings dam failures. https://www.wise-uranium.org/mdaf.html

Yeager, C. L. J., L. W. Harding, and M. E. Mallonee. 2005. Phytoplankton production, biomass and community structure following a summer nutrient pulse in Chesapeake Bay. Aquat. Ecol. **39**: 135–149. doi:10.1007/s10452-004-4767-6

Yoder, J. A. 1979. Effect of temperature on light-limited growth and chemical composition of *Skeletonema-Costatum* (Bacillariophyceae). J. Phycol. **15**: 362–370. doi:10.1111/j.1529-8817.1979.tb00706.x

Zhang, F., M. Li, P. M. Glibert, and S. H. S. Ahn. 2021. A three-dimensional mechanistic model of *Prorocentrum minimum* blooms in eutrophic Chesapeake Bay. Sci. Total Environ. **769**: 144528. doi:10.1016/j.scitotenv.2020.144528

Acknowledgments

The authors thank the two anonymous reviewers for their helpful comments. This work is funded by the National Oceanic and Atmospheric Administration National Centers for Coastal Ocean Science Competitive Research Program under Award NA19NOS4780183. This is ECOHAB contribution number ECO1075 and contribution number 6317 from the University of Maryland Center for Environmental Science.

Conflict of Interest

None declared.

Submitted 20 February 2023
Revised 05 June 2023
Accepted 06 August 2023

Associate editor: Michele A. Burford